Chinese Journal of Electronics
vol. 33, no. 5, pp. 1181–1187, September 2024
https://doi.org/10.23919/cje.2022.00.327

RESEARCH ARTICLE

Investigating the Effects of V_2C MXene on Improving the Switching Stability and Reducing the Operation Voltages of TiO_2-Based Memristors

Nan HE[1], Lei WANG[1], and Yi TONG[1,2]

1. *College of Electronic and Optical Engineering, College of Flexible Electronics (Future Technology), and College of Integrated Circuit Science and Engineering, Nanjing University of Posts and Telecommunications, Nanjing 210023, China*
2. *Gusu Laboratory of Materials, Suzhou 215000, China*

Corresponding author: Yi TONG, Email: tongyi@njupt.edu.cn
Manuscript Received September 28, 2022; Accepted January 28, 2023

Abstract — Three-atoms-type V_2C MXene, an emerging class of transition metal carbides, has attracted tremendous attention in the fabrication of advanced memristive devices due to its excellent electrochemical properties. However, the inserted effects and corresponding physical mechanisms of inserting V_2C on traditional TiO_2-based memristors have not been clearly explored. In this work, exhaustive electrical characterizations of the V_2C/TiO_2-based devices exhibit enhanced performance (e.g., improved switching stability and lower operating voltages) compared to the TiO_2-based counterparts. In addition, the advantaged influences of the inserted V_2C have also been studied by means of first-principles calculations, confirming that V_2C MXene enables controllable internal ionic process and facilitated formation mechanism of the Ag conductive filaments. This work demonstrates a way to combine experimental and theoretical investigations to reveal the positive effects of introducing V_2C MXene on memristor, which is beneficial for fabricating performance-enhanced memristors.

Keywords — Memristor, V_2C MXene, First-principles calculation, Switching stability, Formation mechanism.
Citation — Nan HE, Lei WANG, and Yi TONG, "Investigating the Effects of V_2C MXene on Improving the Switching Stability and Reducing the Operation Voltages of TiO_2-Based Memristors," *Chinese Journal of Electronics*, vol. 33, no. 5, pp. 1181–1187, 2024. doi: 10.23919/cje.2022.00.327.

I. Introduction

Memristor, an ideal device for simulating the artificial synapse, has been undoubtedly considered as one of the fundamental functional building blocks in developing brain-inspired computational systems due to many merits, such as biological structure and functions, good complementary metal-oxide-semiconductor (CMOS) compatibility, and low energy consumption [1]–[3]. The simple metal/insulator/metal (MIM) structure of memristors enables the high-density integration, in which the medium functional materials play the key role in the resistive switching (RS) process from the perspectives of materials [4], [5]. Up to now, titanium dioxide (TiO_2), a binary transition metal oxide, has been widely employed as a dielectric layer to construct memristors due to many remarkable advantages, for example, ease of deposition, high temperature stability, and high dielectric constant [6]–[9]. However, there is still lots of room for the enhancement of some unsatisfactory RS characteristics of TiO_2-based memristor including the large operating voltages and relatively poor endurance property, since the existing crucial obstacles can hinder further development and thus fail to fit industrial requirements.

Recently, five-atoms-type Ti_3C_2 MXene, a hot family of two-dimensional materials, has been inserted into memristors to improve the device performance [10], [11]. In addition, the positive inserted effects of Ti_3C_2 materials have been investigated by the compared electrical RS characteristics and the first-principles calculations. More recently, three-atoms-type V_2C MXene, another new member of MXene family, has been previously introduced into traditional TiO_2-based memristors with structure of

Associate Editor: Prof. Yuchao YANG, Peking University.

Ag/V_2C/TiO_2/W to stimulate electronic synapses since V_2C MXene has more stable atomic structure and higher electronic conductivity when compared to Ti_3C_2 [12], [13]. However, the inserted effects of V_2C MXene on the RS characteristics (e.g., switching stability and operating voltage) have not been intensively investigated so far. More importantly, the corresponding physical mechanisms related to the insertion of V_2C have not been systematically elucidated, which requires considerable effort to explore since a deeper understanding of the RS mechanism will in turn guide the structural design of the device.

In this work, the memristors with and without V_2C MXene have been synchronously fabricated by magnetron sputtering and spin-coating methods. As a comparison, the RS characteristics of both memristors have been investigated in detail from the perspectives of electrical properties, showing that V_2C-based memristors exhibit better performance including longer data retention, more concentrated and lower operating voltages, and more stable endurance characteristics. In addition, by means of first-principles calculations and electrode-cutting operations, their RS mechanisms have been explained by locally controlled formation and dissolution of the Ag conductive filaments (CFs). All in all, our work provides a viable approach to effectively designing the performance-enhanced memristors and further clarifying the underlying mechanisms of the investigated devices.

II. Experiments

The 80 nm W bottom electrodes (BEs) and 60 nm TiO_2 layer (for V_2C/TiO_2-based device) have been sequentially deposited by magnetron sputtering with the respective targets on a cleaned 2-inch wafer. After that, V_2C MXene layer can be prepared by spin-coating (1000 rpm for 60 s) the mixture of V_2C material and dimethyl sulfoxide (DMSO) with a ratio of 10 mg/ml. And finally, 80 nm Ag top electrodes (TEs) were deposited by direct current sputtering to complete the fabrication of the Ag/V_2C/TiO_2/W structure devices. The control TiO_2-based devices without V_2C MXene have been prepared by the similar processes under the same environment.

The electrical RS characteristics of both structural devices have been tested by using Keithley 4200A-SCS. First-principles calculations have been carried out within the framework of density functional theory (DFT), which has been implemented in the Vienna *Ab-Initio* simulation package (VASP) software [14], [15]. Generalized gradient approximation (GGA) of Perdew-Burke-Ernzerhof (PBE) has been employed for computing the exchange-correlation energy. In addition, the valence electronic states have been expanded on the basis of plane-wave with the core-valence interaction represented by adopting the projector augmented wave (PAW) method. More importantly, for all calculations, the plane-wave cut-off energy has been set to 520 eV and a Γ-centered k-mesh of $2 \times 2 \times 2$ has been utilized [16]. Furthermore, electrical convergence can be achieved once the force acting on each ionic was less than 0.02 eV/Å.

III. Results and Discussion

The atomic structure of the as-prepared V_2C MXene has been shown in Figure 1(a), where the unit cell of V_2C consists of three atoms including two vanadium atoms (cyan balls) and one carbon atom (black ball). Figure 1(b) exhibits a schematic configuration of the studied device with Ag/V_2C/TiO_2/W structure. As shown in Figures 1(c) and (d), the typical of current-voltage (*I-V*) curves of the both devices operating at the same compliance current of 400 μA show the similar bipolar RS behaviors. Both devices have a high-resistance state (HRS, OFF-State) in their initial stages and are set to low-resistance state (LRS, ON-State) referred as set process when applying an appropriate positive voltage (i.e., set voltage, V_{Set}). Conversely, both devices can be reversibly reset from the LRS to HRS termed as reset process at a certain voltage (i.e., reset voltage, V_{Reset}) once changing the polarity of the electric field. Compared with the control device without MXene, we found that the lower voltage corresponds to the current jump process of V_2C/TiO_2-based device, as demonstrated in the insets of Figures 1(c) and (d). The current jump process is obtained after increasing the compliance current value and can be functionalized as electroforming process for 400 μA. In addition, the extremely small variation of multiple *I-V* curves reveals the remarkable repeatability of V_2C/TiO_2-based device, strongly reflecting the advantaged effects of introducing V_2C. Such positive impact will be discussed later in greater detail. More obviously, the RS behavior of the TiO_2-based device fails after only 19 cycles, whereas the V_2C/TiO_2-based device can switch for 240 cycles without any manifest fluctuation.

Figures 2(a) and (b) exhibit the cyclic endurance properties of the TiO_2-based and V_2C/TiO_2-based device, respectively. The device's states before and after set process were measured with a low readout voltage of 0.1 V. It is evident that the V_2C/TiO_2-based device performs better endurance, i.e., more stable switching cycles. In addition, the corresponding operating voltages (set voltage and reset voltage) have been replotted with the form of cumulative distributions, as shown in Figures 2(c) and (d). It can be clearly observed that the set voltage (range from 0.62 V to 0.66 V) and reset voltage (from −0.19 V to −0.02 V) of the V_2C/TiO_2-based memristor are lower and more concentrated than the set voltage (range from 0.72 to 1.07 V) and reset voltage (from −0.69 V to −1.55 V) of TiO_2-based device, respectively. Besides, the reset current of as-manufactured V_2C-based device is lower than that of the device without V_2C, revealing the lower power consumption of reset process. Such reduction and concentration with respect to the operating voltages are crucial in pursuing stable and low-power consumption memristors that are more suitable to realize low-power operation [17]. Moreover, retention characteristics at room temperature have been tested to evaluate the memory

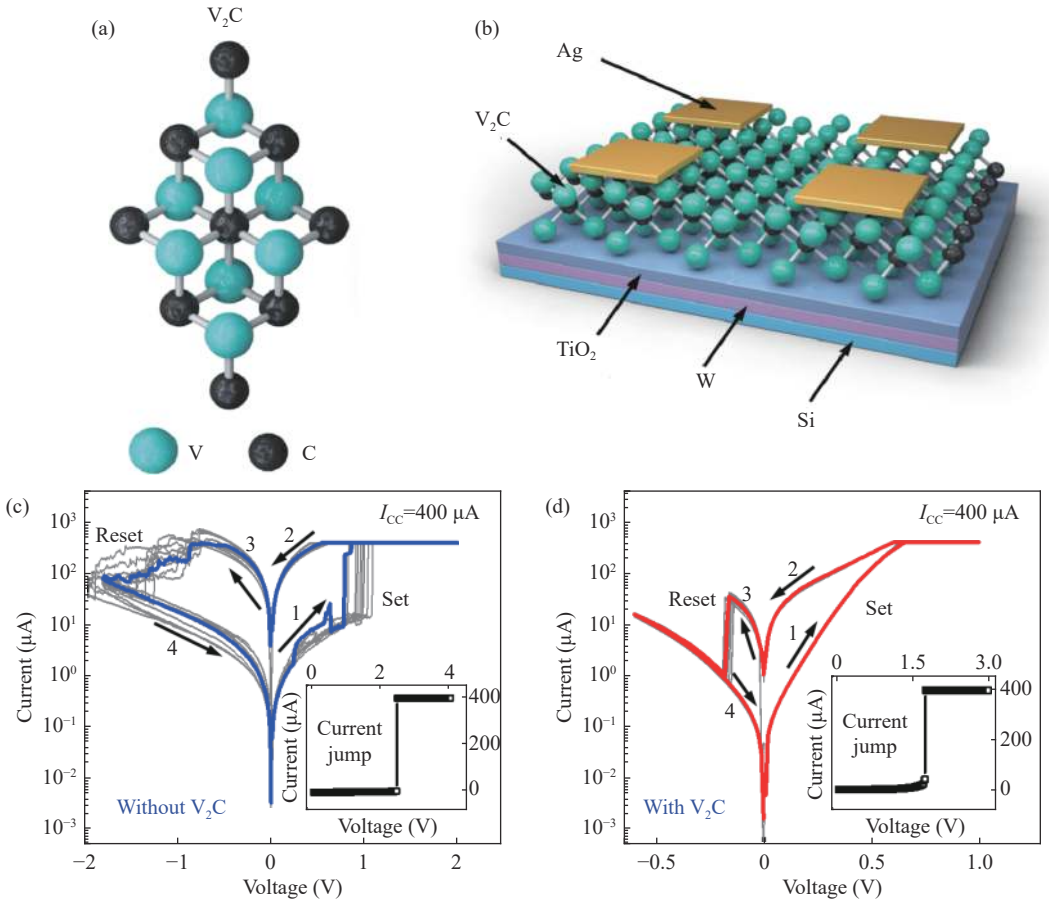

Figure 1 (a) Atomic structure of pristine V_2C MXene; (b) Schematic illustration of the studied Ag/V_2C/TiO_2/W device structure; Typical bipolar RS behaviors for the device (c) Without and (d) With V_2C MXene [12]. The insets represent the current jump behaviors before measuring the typical *I-V* curves.

nonvolatility of two devices, as indicated in Figures 2(e) and (f). The V_2C/TiO_2-based memristor demonstrates better retention performance since the HRS of TiO_2-based memristor has obvious decay phenomenon in a very short time. The large fluctuation may be due to the stochastic nature of positively charged Ag ions migration and diffusion in TiO_2 layer during the RS process [18].

Moreover, the statistical HRS and LRS distributions for randomly selected four devices from conventional TiO_2-based and V_2C-inserted memristors have been plotted with box plots, as demonstrated in Figures 2(g) and (h), respectively. The results show that extracted HRS and LRS values of V_2C-based devices fluctuate within a relatively narrow range. The statistical analysis of what percentage of devices showed enhanced performance will be carried out in our future study. Detailed comparisons performed above disclose that the insertion of V_2C is significant for the reduction of operating voltages and enhancement of RS stability. The RS characteristics of the as-fabricated V_2C-based memristors and other as-investigated devices recently reported in the literature are compared and summarized in Table 1, suggesting the relatively excellent performance of the studied V_2C-based memristors [19]–[34].

For the sake of investigating why the inserted V_2C-based memristors can obtain low concentrated operating voltages and more stable RS stability, formation energies calculations related to the formation of Ag CFs as well as differential charge density analyses with respect to the electronic exchange have been carried out via the first-principles calculations, as presented in Figure 3 [35], [36]. Structural models of the TiO_2 compound and V_2C/TiO_2 heterojunction have been modeled in a single unit respectively, where C, O, Ag, V, and Ti atoms are represented by gray, red, dark blue, purple, and light blue balls, respectively. As a result, the substitution of Ti site by Ag at low temperature requires a relatively large formation energy of 0.97 eV in the single-layer TiO_2-based memristor, whereas the Ag substitution in V_2C/TiO_2 heterojunction is strongly facilitated with a lower formation energy of 0.63 eV, as plotted in Figures 3(a) and (c) respectively. Such reduction fact implies that the V_2C/TiO_2-based memristor has higher structural stability to easily initialize the formation of Ag clusters. After the initialization of Ag clusters, the final Ag CFs are easily formed and the memristor is switched-ON.

In order to achieve a deeper understanding of the facilitated formation mechanisms of Ag dopants at V_2C/TiO_2 heterojunctions, the differential charge density distribution and Bader charge analysis have been exe-

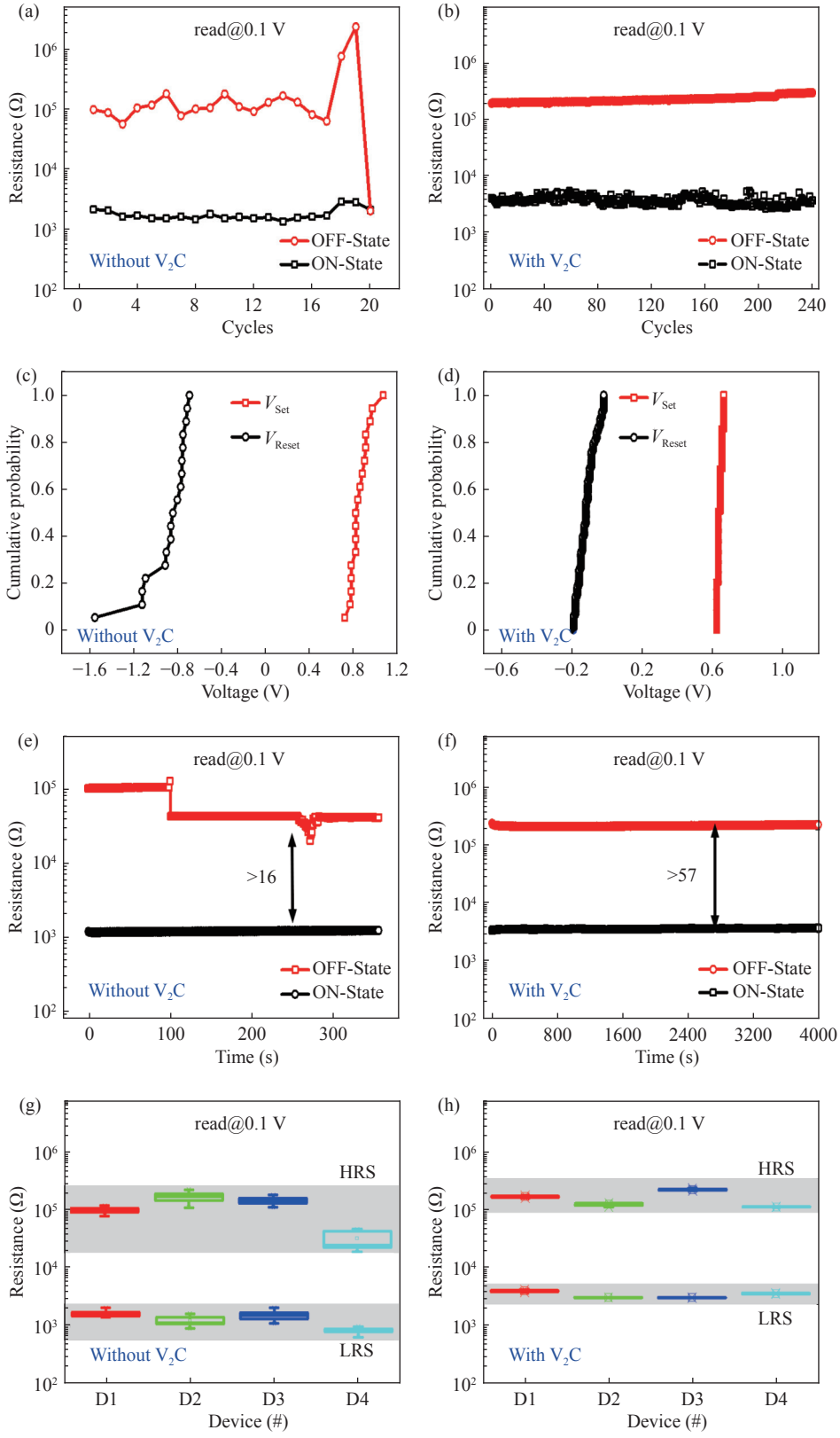

Figure 2 Cyclic endurance property of the device (a) Without and (b) With V_2C MXene. Cumulative probability distributions of the operation voltages of the device (c) Without and (d) With V_2C MXene [12]. Data retention characteristics of the device (e) Without and (f) With V_2C MXene [12]. Device-to-device distributions of HRS and LRS read at 0.1 V for four devices (g) Without and (h) With V_2C MXene.

cuted in Figures 3(b) and (d) for the corresponding formation energies (i.e., 0.97 eV and 0.63 eV) of the two structures, respectively. In comparison with the result of TiO_2-based memristor in Figure 3(b), there exists

Table 1 Comparison of few recently reported memristors with our customized devices

Reference	Material	V_{Set} (V)	V_{Reset} (V)	Cycles	Retention (s)
Ours	V_2C/TiO_2	0.62–0.66	−0.02 to −0.19	240	4×10^3
[20]	ZnO NPs/CuO NWs	1.5	−0.9	100	8×10^3
[21]	CdSe QDs-PVP	1.6	−1.7	4000	3.8×10^3
[22]	HfO_x/AlO_y	0.8	−1.4	100	1×10^4
[23]	SiC	2.5	−1	100	1×10^3
[24]	$CsPbBr_3$ QDs:GO	2.28	−2.04	500	5×10^3
[25]	SiO_x	1.2	−1.1	100	1×10^4
[26]	Graphene oxide GO	1.8–2.8	−1.6 to −2.6	100	1×10^4
[27]	HfO_2/ZnO	>2.8	<−1	100	1×10^4
[28]	Polydopamine	2.1	−2.3	30	N/A
[29]	Bi_2O_2Se/Bi_2SeO_x	1–2.2	−0.4 to −1.2	20	5×10^3
[30]	LSMO/ZnO	1.4–1.7	−3.1 to −3.3	80	4×10^3
[31]	Mn-ZnO	0.71	−0.6	80	N/A
[32]	$Cs_2BiAgBr_6$	1.0	−0.4	110	1×10^3
[33]	$CsPbBr_3$	−0.2	1.7	100	1×10^4
[34]	TaO_x/Al_2O_3	>2.5	<−2	100	2.5×10^3

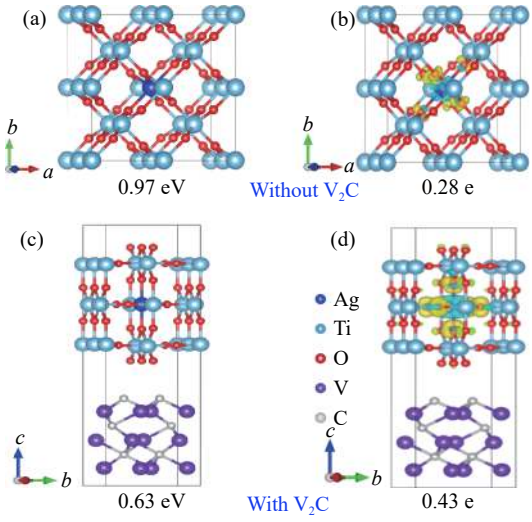

Figure 3 Structural models and required formation energies of (a) Ag-doped TiO_2 compounds and (c) Ag-doped V_2C/TiO_2 heterojunctions; Differential charge density diagrams of the device (b) Without and (d) With V_2C MXene, corresponding to the formation energies (0.97 eV and 0.63 eV) of the initially formed Ag clusters in (a) and (c) respectively. (Ti, O, Ag, V, and C atoms are represented by light blue, red, dark blue, purple, and gray balls, respectively).

stronger charge transfer (larger Bader charge 0.43 e) in V_2C/TiO_2 heterojunctions in Figure 3(d) between Ag ions and their coordinated atoms. Such powerfully reveals that the insertion of V_2C can readily adsorb Ag ions to move and significantly benefit the formation of Ag clusters or CFs as a result of the stronger electrostatic interactions, thus leading to the lower operating voltages and more stable RS behaviors. In other words, the inserted V_2C MXene has a strong capability to easily attract Ag ions to directionally migrate towards the TiO_2 layer along the location of V_2C nanostructures with lower voltage.

To verify the localized formation of CFs rather than uniform distribution in V_2C/TiO_2-based memristor, TE-cutting operations have been experimentally performed, as presented in Figure 4. First, both devices were switched to nonvolatile LRS, and the device's states before and after set process were measured with a low read-out voltage of 0.1 V, as presented in Figure 4(a). After that, the Ag TEs were cut into two parts marked with TE1 and TE2 respectively by using the test probe, as displayed in Figure 4(b). Next, the device's states of both parts have been read, and the results have been plotted in Figures 4(c) and (d). It can be clearly seen that both memristors demonstrate localized formation of CFs (mainly occurring in the right TE1) but the V_2C/TiO_2-based device obviously shows better similarity of LRS read before and after cutting. Such an approach further reveals that the insertion of V_2C MXene can guide the stable creation of CFs because of the lower formation energy and higher charge transfer. On the basis of above theoretical analysis, the schematic diagrams of RS mechanism related to the electrochemical formation of Ag CFs have been proposed and illustrated in Figure 5, where the distribution of CFs in TiO_2-based device is relatively stochastic. In the near future, the X-ray photoelectron spectroscopy (XPS) or transmission electron microscopy (TEM) characterization methods will be employed to future prove the internal mechanism of our studied devices.

IV. Conclusion

In conclusion, the compared results presented here

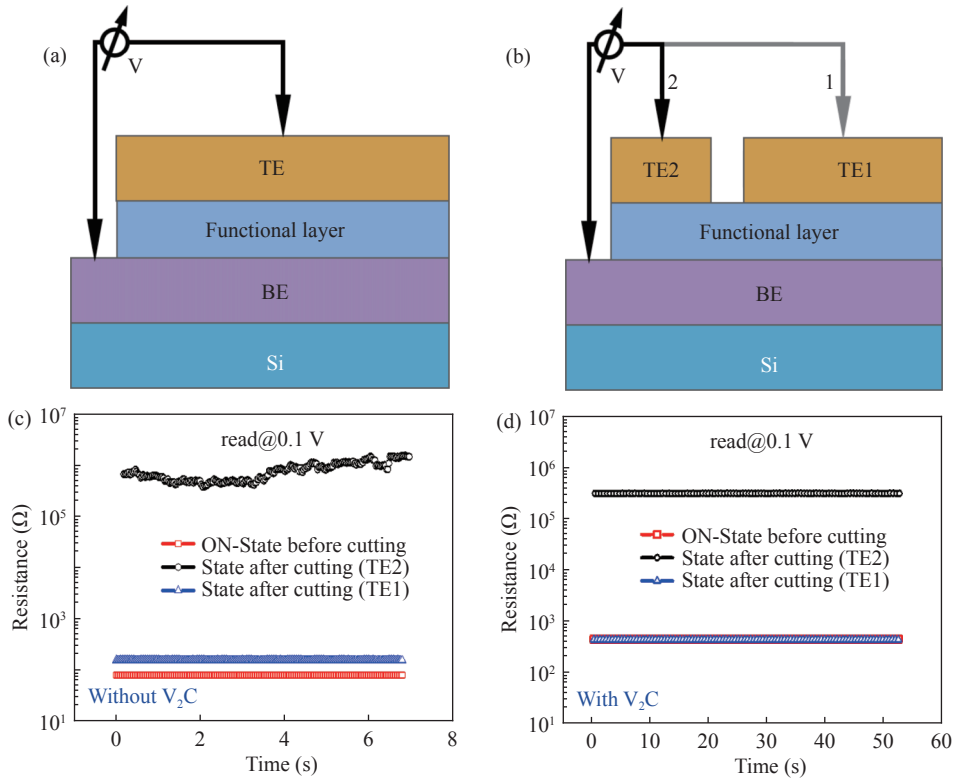

Figure 4 Schematic illustrations of (a) Before and (b) After electrode-cutting operations; Device states read before and after electrode-cutting operations of the device (c) Without and (d) With V_2C MXene.

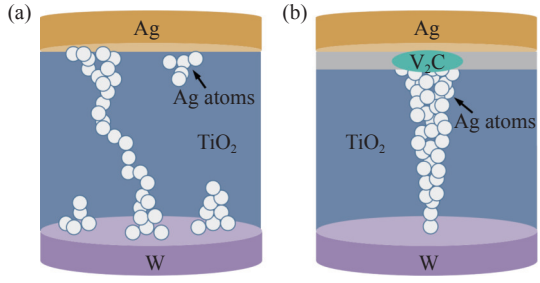

Figure 5 Schematic illustrations of resistive switching mechanisms of the device (a) Without and (b) With V_2C MXene.

experimentally exhibit that three-atoms-type V_2C MXene can be introduced into conventional TiO_2-based memristors to improve the switching stability and reduce the operating voltages. In addition, the favorable formation energy, differential charge density distribution, and Bader charge analysis based on first-principles calculations not only theoretically reveal that the V_2C/TiO_2-based device has higher structural stability, but also clearly interpret the corresponding facilitated formation mechanisms.

Acknowledgements

This work was supported by the 2030 Major Project of the Chinese Ministry of Science and Technology (Grant No. 2021ZD0201200), the High-End Foreign Experts Project of the Ministry of Science and Technology (Grant No. G2022178034L), the Postgraduate Research and Practice Innovation Program of Jiangsu Province (Grant Nos. KYCX190956 and 4600KYCX220928), and the Jiangsu Province Research Foundation (Grant Nos. BK20191202 and 16KJA510003).

References

[1] K. M. Leng, X. Y. Yu, Z. Y. Ma, *et al.*, "Artificial synapse arrays based on SiO_x/TiO_x memristive crossbar with high uniformity for neuromorphic computing," *Applied Physics Letters*, vol. 120, no. 4, article no. 043101, 2022.

[2] J. Bera, A. Betal, A. Sharma, *et al.*, "CdSe quantum dot-based nanocomposites for ultralow-power memristors," *ACS Applied Nano Materials*, vol. 5, no. 6, pp. 8502–8510, 2022.

[3] N. He, L. Y. Tao, Q. Q. Zhang, *et al.*, "Reversible transition of volatile and nonvolatile switching in Ag—In—Zn—S quantum dot-based memristors with low power consumption for synaptic applications," *ACS Applied Nano Materials*, vol. 4, no. 3, pp. 2365–2374, 2021.

[4] Y. R. Niu, K. Jiang, X. Y. Dong, *et al.*, "High performance and low power consumption resistive random access memory with $Ag/Fe_2O_3/Pt$ structure," *Nanotechnology*, vol. 32, no. 50, article no. 505715, 2021.

[5] W. C. Jhang and C. C. Hsu, "Coexistence of nonvolatile WORM, bipolar, unipolar, and volatile resistive switching characteristics in a dry oxide layer with Ag conductive bridges," *IEEE Transactions on Electron Devices*, vol. 69, no. 9, pp. 4914–4919, 2022.

[6] D. Acharyya, A. Hazra, and P. Bhattacharyya, "A journey towards reliability improvement of TiO_2 based resistive random access memory: A review," *Microelectronics Reliability*, vol. 54, no. 3, pp. 541–560, 2014.

[7] J. M. Won, M. S. Kim, and S. C. Hong, "The cause of deactivation of VO_x/TiO_2 catalyst by thermal effect and the role of tungsten addition," *Chemical Engineering Science*, vol. 229, article no. 116068, 2021.

[8] D. H. Kwon, K. M. Kim, J. H. Jang, *et al.*, "Atomic structure of conducting nanofilaments in TiO_2 resistive switching memory," *Nature Nanotechnology*, vol. 5, no. 2, pp. 148–153, 2010.

[9] D. P. Sahu and S. N. Jammalamadaka, "Remote control of resistive switching in TiO_2 based resistive random access

memory device," *Scientific Reports*, vol. 7, article no. 17224, 2017.
[10] X. J. Lian, X. Y. Shen, M. C. Zhang, *et al.*, "Resistance switching characteristics and mechanisms of MXene/SiO_2 structure-based memristor," *Applied Physics Letters*, vol. 115, no. 6, article no. 063501, 2019.
[11] X. J. Lian, J. K. Fu, Z. X. Gao, *et al.*, "High-performance artificial neurons based on Ag/MXene/GST/Pt threshold switching memristors," *Chinese Physics B*, vol. 32, no. 1, article no. 017304, 2023.
[12] N. He, Q. Q. Zhang, L. Y. Tao, *et al.*, "V_2C-based memristor for applications of low power electronic synapse," *IEEE Electron Device Letters*, vol. 42, no. 3, pp. 319–322, 2021.
[13] X. T. Chen, Y. Wang, D. Q. Shen, *et al.*, "First-principles calculation and experimental investigation of a three-atoms-type MXene V_2C and its effects on memristive devices," *IEEE Transactions on Nanotechnology*, vol. 20, pp. 512–516, 2021.
[14] G. Kresse and J. Furthmüller, "Efficient iterative schemes for *ab initio* total-energy calculations using a plane-wave basis set," *Physical Review B*, vol. 54, no. 16, pp. 11169–11186, 1996.
[15] J. Perdew, K. Burke, and M. Ernzerhof, "Generalized gradient approximation made simple," *Physical Review Letters*, vol. 77, no. 18, pp. 3865–3868, 1996.
[16] P. E. Blöchl, "Projector augmented-wave method," *Physical Review B*, vol. 50, no. 24, pp. 17953–17979, 1994.
[17] X. B. Yan, Q. L. Zhao, A. P. Chen, *et al.*, "Vacancy-induced synaptic behavior in 2D WS_2 nanosheet-based memristor for low-power neuromorphic computing," *Small*, vol. 15, no. 24, article no. 1901423, 2019.
[18] Q. Xue, Y. Peng, L. Cao, *et al.*, "Ultralow set voltage and enhanced switching reliability for resistive random-access memory enabled by an electrodeposited nanocone array," *ACS Applied Materials & Interfaces*, vol. 14, no. 22, pp. 25710–25721, 2022.
[19] X. B. Yan, Y. F. Pei, H. W. Chen, *et al.*, "Self-assembled networked PbS distribution quantum dots for resistive switching and artificial synapse performance boost of memristors," *Advanced Materials*, vol. 31, no. 7, article no. 1805284, 2019.
[20] Y. Q. Wang, W. X. Wang, C. W. Zhang, *et al.*, "A digital—analog integrated memristor based on a ZnO NPs/CuO NWs heterostructure for neuromorphic computing," *ACS Applied Electronic Materials*, vol. 4, no. 7, pp. 3525–3534, 2022.
[21] R. R. Pradhan, J. Bera, A. Betal, *et al.*, "Hot injection-based synthesized colloidal CdSe quantum dots embedded in poly(4-vinylpyridine) (PVP) matrix form a nanoscale heterostructure for a high on—off ratio memory-switching device," *ACS Applied Materials & Interfaces*, vol. 13, no. 21, pp. 25064–25071, 2021.
[22] C. X. Wang, G. Q. Mao, M. H. Huang, *et al.*, "HfO_x/AlO_y superlattice-like memristive synapse," *Advanced Science*, vol. 9, no. 21, article no. 2201446, 2022.
[23] O. Kapur, D. K. Guo, J. Reynolds, *et al.*, "Back-end-of-line SiC-based memristor for resistive memory and artificial synapse," *Advanced Electronic Materials*, vol. 8, no. 9, article no. 2200312, 2022.
[24] X. M. Liu, S. X. Ren, Z. H. Li, *et al.*, "Flexible transparent high-efficiency photoelectric perovskite resistive switching memory," *Advanced Functional Materials*, vol. 32, no. 38, article no. 2202951, 2022.
[25] M. Park, J. Park, and S. Kim, "Compatible resistive switching mechanisms in Ni/SiO_x/ITO and application to neuromorphic systems," *Journal of Alloys and Compounds*, vol. 903, article no. 163870, 2022.
[26] H. S. Choi, J. Lee, B. Kim, *et al.*, "Highly-packed self-assembled graphene oxide film-integrated resistive random-access memory on a silicon substrate for neuromorphic application," *Nanotechnology*, vol. 33, no. 43, article no. 435201, 2022.
[27] W. Zhang, J. Z. Lei, Y. X. Dai, *et al.*, "Switching-behavior improvement in HfO_2/ZnO bilayer memory devices by tailoring of interfacial and microstructural characteristics," *Nanotechnology*, vol. 33, no. 25, article no. 255703, 2022.
[28] J. Yun and D. Kim, "Unraveling the role of polydopamines in resistive switching in Al/Polydopamine/Al structure for organic resistive random-access memory," *Polymers*, vol. 14, no. 15, article no. 2995, 2022.
[29] Y. Xia, J. Wang, R. Chen, *et al.*, "2D heterostructure of Bi_2O_2Se/Bi_2SeO_x nanosheet for resistive random access memory," *Advanced Electronic Materials*, vol. 8, no. 9, article no. 2200126, 2022.
[30] K. Kumari, S. Kar, A. D. Thakur, *et al.*, "Role of an oxide interface in a resistive switch," *Current Applied Physics*, vol. 35, pp. 16–23, 2022.
[31] Q. Xue, T. Hang, J. H. Liang, *et al.*, "Nonvolatile resistive memory and synaptic learning using hybrid flexible memristor based on combustion synthesized Mn-ZnO," *Journal of Materials Science and Technology*, vol. 119, no. 24, pp. 123–130, 2022.
[32] X. Y. Wang, N. Ali, G. Bi, *et al.*, "Investigation of resistive switching in lead-free bismuth–silver halide double perovskite," *Semiconductor Science and Technology*, vol. 37, no. 6, article no. 065011, 2022.
[33] G. Abbas, M. Hassan, Q. Khan, *et al.*, "A low power-consumption and transient nonvolatile memory based on highly dense all-inorganic perovskite films," *Advanced Electronic Materials*, vol. 8, no. 9, article no. 2101412, 2022.
[34] X. Y. Zhao, K. L. Zhang, K. Hu, *et al.*, "Self-rectifying Al_2O_3/TaO_x memristor with gradual operation at low current by interfacial layer," *IEEE Transactions on Electron Devices*, vol. 68, no. 12, pp. 6100–6105, 2021.
[35] V. I. Ivashchenko, P. E. A. Turchi, V. I. Shevchenko, *et al.*, "Stability and mechanical properties of molybdenum carbides and the Ti–Mo–C solid solutions: A first-principles study," *Materials Chemistry and Physics*, vol. 275, article no. 125178, 2022.
[36] X. M. He, J. C. Hu, and X. Tian, "Electronic characteristics of PbS quantum dots passivated by halides on different surfaces," *Applied Surface Science*, vol. 568, article no. 150736, 2021.

Nan HE received the B.S. degree in microelectronics from Nanjing University of Posts and Telecommunications, Nanjing, China, and is now a Ph.D. candidate with the College of Electronic and Optical Engineering, and the College of Flexible Electronics (Future Technology), Nanjing University of Posts and Telecommunications, Nanjing, China. His current research interests include stable and high-performance memristive devices design.
(Email: 2020020117@njupt. edu.cn)

Lei WANG received the Ph.D. degree in 2009 at University of Exeter, Exeter, UK. Between 2008 and 2011, he was employed as a Postdoctoral Research Fellow with University of Exeter, Exeter, UK to work on a fellowship funded by European Commission. In 2020, he joined Nanjing University of Posts and Telecommunications, Nanjing, China, as a full Professor. His research interests include phase-change memories, neural networks, and other phase-change based optoelectronic devices and their potential applications.
(Email: LeiWang1980@njupt.edu.cn)

Yi TONG received the Ph.D. degree from National University of Singapore, Singapore, Singapore, in 2014. He is now a Professor with the College of Integrated Circuit Science and Engineering, Nanjing University of Posts and Telecommunications. His current research interest include post-CMOS hardware for in-memory computing, neuromorphic computing, and artificial intelligence.
(Email: tongyi@njupt.edu.cn)